Mechanism and Nanosize Products of the Sol−Gel Reaction Using Diphenylsilanediol and 3-Methacryloxypropyltrimethoxysilane as Precursors

Se Yun Kim,[†] Saji Augustine,[†] Young Joo Eo,[†] Byeong Soo Bae,[†] Seong Ihl Woo,[‡] and Jeung Ku Kang*[,†]

Department of Materials Science and Engineering and Department of Chemical and Biomolecular Engineering and Center for Ultramicrochemical Process Systems, KAIST, Daejon 305-701, Republic of Korea

Received: December 23, 2004; In Final Form: March 14, 2005

We use a first-principles calculation and small-angle neutron scattering (SANS) to investigate the mechanism and the nanosize products of the sol−gel reaction with diphenylsilanediol (DPD) and 3-methacryloxypropyltrimethoxysilane (MEMO) precursors in synthesizing a hybrid waveguide material. It is predicted that switching between a DPD hydroxyl and a MEMO methoxy with a reaction rate of 6.8×10^{-6} s^{-1} at 300 K is the fastest process for the first reaction step, thus generating diphenylmethoxysilanol (DPM) and 3-methacryloxypropyldimethoxysilanol (MEDO) as products. However, we determine that this reaction pathway could be modified by the presence of the H_2O released from a catalyst such as $Ba(OH)_2 \cdot H_2O$. Next, switching between the DPM hydroxyl and the MEDO methoxy is followed to generate diphenyldimethoxysilane (DPDM) and 3-methacryloxypropylmethoxysilanediol (MEMDO). However, condensation between a MEMDO hydroxyl and a DPDM methoxy is found to be most favorable for the third reaction step, which generates the DPDM−MEMDO dimer and CH_3OH molecule as products. In a similar fashion, a DPDM methoxy of the DPDM−MEMDO dimer can condense with a MEMDO hydroxyl of the second DPDM−MEMDO dimer to increase the chain, but its reaction rate of 2.8×10^{-11} s^{-1} is predicted to be about 5 times smaller than that between a DPDM methoxy and a MEMDO hydroxyl. This implies that the reaction rate for the larger nanostructures becomes smaller. Additionally, our SANS measurements determine that the final products from our sol−gel reaction are on the nanometer scale, at sizes from 1.76 to 2.36 nm.

I. Introduction

There is great interest in designing the ideal waveguide materials for optical applications. Conventional waveguides are made of inorganic glasses[1,2] and organic polymers.[3,4] However, there still remain considerable challenges to reducing optical losses and giving them good adhesion on various substrates, high thermal stability, and low processing temperatures. Recently, hybrid materials[5−7] with both organic and inorganic components have been proposed as good candidates for satisfying the ideal properties and processing conditions simultaneously. In addition, the synthesis of the hybrid materials with nanometer-scale sizes is also important in making fine nanostructures and in getting homogeneous properties within a waveguide.

Both hydrolytic and non-hydrolytic processes have been proposed to produce the hybrid materials. However, hybrid materials synthesized by hydrolytic processes have more optical losses than those synthesized by non-hydrolytic processes.[8−11] This is because hydrolytic processes[12,13] generally generate more undesired hydroxyls that are sensitive to vibrational excitations. The non-hydrolytic synthesis of hybrid materials consists of a two-step process.[14] In the first step, the precursors are linked to produce siloxane (−Si−O−Si−) bridges, and the second step involves cross linking between organic side chains of the inorganic structures in a 3D network by UV light. However, depending on the nature of the interface between organic and inorganic elements in hybrid materials, they are classified into two different groups.[15,16] One group has their organic and inorganic components linked through van der Waals or hydrogen bonding, and the other group has its network formed through covalent or ionic bonding.

Buestrich et al.[7] and Houbertz et al.[17,18] synthesized a hybrid material from the sol−gel reactions[19] using diphenylsilanediol (DPD) and 3-methacryloxypropyltrimethoxysilane (MEMO) precursors. A combination of DPD, having OH groups for non-hydrolytic processes, with MEMO, enabling the resulting materials to be patterned by UV, provides a good precursor system. Their IR study[7] shows that there is no SiO−H stretching mode (3600−3200 cm^{-1}) in their synthesized hybrid material that results in low scattering losses (0.3 dB/cm at 1320 nm and 0.6 dB/cm at 1550 nm). It has also good adhesion on a silicon substrate and a relatively low processing temperature of 150 °C. However, detailed thermodynamic and kinetic parameters for intermediate nanostructures likely to be produced from the reactions using DPD and MEMO precursors are not reported. Also, there still remains considerable ambiguity as to whether the final products from the sol−gel reaction could be on the nanometer scale.

Here, we use a first-principles calculation[20−22] and small-angle neutron scattering (SANS) methods to determine the mechanisms and intermediate nanostructures for the sol−gel processes using DPD and MEMO precursors. First, we investigate condensation reactions between two DPDs, between one

* Corresponding author. E-mail: jeungku@kaist.ac.kr. Tel: +82-42-869-3338. Fax: +82-42-869-3310.

[†] Department of Materials Science and Engineering.

[‡] Department of Chemical and Biomolecular Engineering and Center for Ultramicrochemical Process Systems.

10.1021/jp044151q CCC: $30.25
Published on Web 04/12/2005

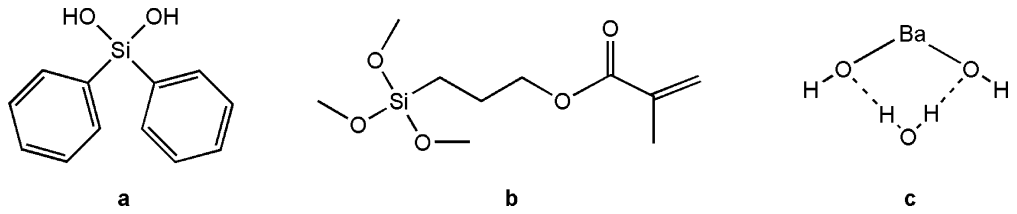

Figure 1. Reactants and the catalyst: (a) DPD (diphenylsilanediol) and (b) MEMO (3-methacryloxypropyltrimethoxysilane) and (c) $Ba(OH)_2 \cdot H_2O$.

DPD and one MEMO, and between two MEMOs. Also, the switching reaction between one DPD hydroxyl and one MEMO methoxy is explored, which generates diphenylmethoxysilanol (DPM) and 3-methacryloxypropyldimethoxysilanol (MEDO) as products. Then, the catalytic effects by the H_2O released from a catalyst such as $Ba(OH)_2 \cdot H_2O$ are additionally investigated because they could play an important role in reducing the reaction barrier as reported in the previous studies.[23−25] Moreover, the reactions by DPM and MEDO molecules are explored. Next, we investigate the reactions by the diphenyldimethoxysilane (DPDM) and 3-methacryloxypropylmethoxysilanediol (MEMDO) molecules as well as the reactions by the dimer (DPDM−MEMDO) molecules. Last, the sizes of the final products are determined on the basis of experimental SANS measurements and theoretical predictions.

These results are reported and discussed in section III. Section II provides some details about the calculations, and section IV summarizes our results.

II. Computational Details

All calculations are performed using the self-consistent B3LYP[20] and KMLYP[21] density functional theories and using the QCISD[22] level of theory. The B3LYP was shown to predict accurate geometries and thermochemical data compared to other generalized gradient approximations (GGAs)[26−30] and local density approximations (LDAs),[31,32] whereas KMLYP was proven to be more accurate in predicting transition-state barriers[21,33,34] than other DFT methods.

The electronic wave function is expanded using the 6-31G valence double-ζ[35] basis set and the 6-311+G(d,p) valence diffuse triple-ζ plus polarization[35] basis set. In this study, the full optimizations of all geometry parameters for reactants, transition states, and products are performed at the B3LYP/6-31G level of theory, and then the enthalpies of reactions and transition-state barriers are obtained using the KMLYP/6-311+G(d,p) single-point energies determined at the B3LYP geometries. All calculations are performed with Gaussian 03.[36]

We use DPD and MEMO precursors to make siloxane bridges. DPD consists of one silicon atom, two hydroxyls, and two phenyl groups. The valence orbitals for the silicon atom are sp^3-hybridized, and they bond to two phenyl and two hydroxyl fragments as shown in Figure 1a. Our predicted DPD Si−OH bond length of 1.64 Å is found to be in close agreement with the experimental values of 1.63−1.64 Å.[37,38] In addition, the DPD Si−phenyl bond length of 1.89 Å is calculated to be consistent with the QCISD value of 1.90 Å. The MEMO molecule has one 3-methacryloxypropyl group and three methoxy groups around the silicon atom as described in Figure 1b. In all possible sol−gel processes using the DPD and MEMO precursor system, the Si−OH fragments of the DPD and the $Si-OCH_3$ fragments of the MEMO are active groups that form a siloxane bridge (−Si−O−Si−), thereby releasing H_2O or CH_3-OH as a byproduct.

III. Results and Discussion

A. Reaction Mechanism and Resulting Nanostructures. By computing the partition functions for the reactants and the transition state, the reaction rate k^{TST} of the canonical rate equation[39] is determined by

$$k^{TST} = \Gamma(T)\frac{k_B T}{h}\frac{Q_{TS}}{Q_A Q_B}\exp\left(\frac{-\Delta E_0}{k_B T}\right)$$

where $\Gamma(T)$ is the thermal tunneling coefficient,[21] k_B is the Boltzmann constant, h is the Plank constant, Q_{TS} is the partition function for the transition state, Q_A and Q_B are the partition functions for reactants A and B, and ΔE_0 is the barrier height. We determine the sequence of the reactions by comparing the calculated reaction rates.

There are three plausible cases for condensation in the first step of the sequence, which include reactions between (1) two DPDs, (2) one DPD and one MEMO, and (3) two MEMOs. The first case begins by the initial attack of one DPD hydroxyl on another DPD hydroxyl and then proceeds through the four-centered transition state as shown in Figure 2a. The predicted barrier is 14.9 kcal/mol. Additionally, we find that the 14.9 kcal/mol barrier is also consistent with the 14.4 kcal/mol barrier determined for the KMLYP/6-31G geometries and the 13.9 kcal/mol barrier determined for the KMLYP/6-311+G(d,p) geometries. These results indicate that the KMLYP/6-311+G(d,p)//B3LYP/6-31G energies are proper for an accurate prediction of the transition-state barriers. The second condensation case can occur through two different reaction pathways. The first type is the attack of a DPD hydroxyl on a MEMO methoxy (Figure 2b), whereas the second one is the attack of a MEMO methoxy on a DPD hydroxyl (Figure 2c). However, the first type having the smaller barrier of 15.1 kcal/mol is found to be more favorable. Figure 2d describes the condensation reaction between two MEMOs, but its barrier of 69.3 kcal/mol is predicted to be relatively high compared to those of the two other cases. Recently, Buestrich and co-workers[7] proposed one plausible reaction mechanism for the sol−gel reaction under the DPD and MEMO precursor system. According to their mechanism, first one DPD hydroxyl should condense with one MEMO methoxy to form the DPD−MEMO product having one siloxane bridge, and CH_3OH should also be generated as a byproduct. Then, the CH_3OH would condense with the DPD side in the DPD−MEMO to substitute its hydroxyl with the methoxy group. In this respect, the DPD side could remove its hydroxyl group. However, there could be an alternative pathway to remove hydroxyl groups in the DPD. If switching between a DPD hydroxyl and a MEMO methoxy could consecutively take place twice, then the DPD could remove its two hydroxyl groups. Moreover, our calculations indicate that switching between a DPD hydroxyl and a MEMO methoxy is most likely to occur in the first reaction step because the switching reaction is predicted to have a rate of 6.80×10^{-6} s^{-1} at 300 K, which is much larger than the rates of 3.77×10^{-9} and 1.81×10^{-10}

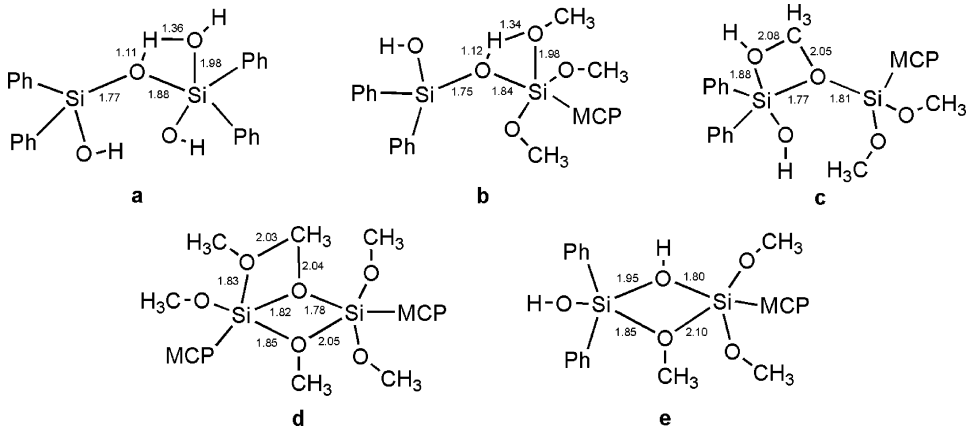

Figure 2. B3LYP/6-31G transition-state geometries for condensations between (a) a DPD hydroxyl on a DPD hydroxyl, (b) a DPD hydroxyl on a MEMO methoxy, (c) a MEMO methoxy on a DPD hydroxyl, and (d) a MEMO methoxy on a MEMO methoxy as well as for the switching reaction between (e) a DPD hydroxyl and a MEMO methoxy. Ph and MCP indicate phenyl and methacryloxypropyl groups, respectively. Bond lengths are in angstroms.

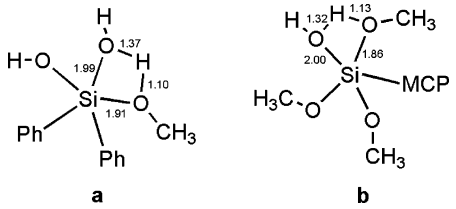

Figure 3. B3LYP/6-31G transition-state geometries for condensations between (a) a DPD and a CH_3OH and (b) a MEMO and a H_2O. Ph and MCP indicate phenyl and methacryloxypropyl groups, respectively. Bond lengths are in angstroms.

s^{-1} for condensations, respectively, between two DPDs and between one DPD and one MEMO. For the switching reaction, the concerted attacks of a DPD hydroxyl on a MEMO silicon and of a MEMO methoxy on a DPD silicon are determined to generate DPM (DPD hydroxyl substituted with one methoxy) and MEDO (MEMO methoxy substituted with one hydroxyl) as products. For the transition state, the DPD Si−OH bond (1.95 Å) is significantly broken while a MEMO Si−OH bond is being formed as shown in Figure 2e. Simultaneously, the Si−OCH_3 bond begins to form on the DPD side, whereas the MEMO Si−OCH_3 bond length of 2.10 Å indicates a considerable amount of the bond being broken.

We also explore the reactions by the byproducts of H_2O and CH_3OH molecules resulting from condensations between two molecules of DPD and MEMO. There exist four types of these reactions. The first type is condensation between one DPD hydroxyl and one CH_3OH (Figure 3a), generating H_2O and DPM as products with a barrier of 19.8 kcal/mol. The condensation reaction between the MEMO methoxy and the H_2O as shown in Figure 3b is the second type, and it is determined to produce CH_3OH and MEDO with a barrier of 19.0 kcal/mol. However, its endothermic enthalpy of 0.6 kcal/mol indicates that it is thermodynamically unfavorable to occur. Figure 4 describes the products from the reactions of CH_3OH or H_2O with the terminal C═C and C═O bonds in the MEMO, but it is found that the barriers of 35.3 to 91.4 kcal/mol by CH_3OH (the third type) and the barriers of 40.4 to 141.7 kcal/mol by H_2O (the fourth type) are considerably high as compared to those for the first and second types. The largest reaction rate of 6.45×10^{-12} s^{-1} is obtained from the first type among these four types. However, this reaction rate is found to be much smaller than 6.80×10^{-6} s^{-1} for the switching reaction between one DPD hydroxyl and one MEMO methoxy. In this respect, the most plausible products from the first reaction step are considered to be DPM and MEDO molecules resulting from the fastest switching process.

There are 10 possible cases for condensation in the second reaction step, which includes the reactions between two DPM hydroxyls, between one DPM hydroxyl and one DPM methoxy, between two DPM methoxys, between one DPM hydroxyl and one MEDO hydroxyl, between one DPM methoxy and one MEDO hydroxyl, between one DPM hydroxyl and one MEDO methoxy, between one DPM methoxy and one MEDO methoxy, between two MEDO hydroxyls, between one MEDO hydroxyl and one MEDO methoxy, and between two MEDO methoxys. All calculated transition barriers and enthalpies are summarized in Table 1. Among these reactions, the attack of a DPM hydroxyl on a MEDO methoxy, whose transition state structure is shown in Figure 5a, is found to have the largest rate of 1.12×10^{-8} s^{-1}. However, the switching reaction between a DPM hydroxyl and a MEDO methoxy, generating DPDM and MEMDO as products, is determined to have a much larger rate of 4.61×10^{-7} s^{-1} than those for condensation. In this respect, the switching reaction is determined to be the fastest process in the second reaction step. The transition state for the switching reaction involves several simultaneous bond breakings and formations: (1) a DPM Si−OH bond being broken with an elongated bond length of 1.82 Å, (2) a Si−OH bond of 1.84 Å formed between a DPM hydroxyl and a MEDO silicon, (3) a Si−OCH_3 bond being broken with the elongated 1.94 Å on the MEDO side, and (4) a Si−OCH_3 of 2.03 Å formed on the DPM side as shown in Figure 5b.

DPDM and MEMDO are the products from the switching reaction in the second reaction step. There exist three possible condensation reactions by these molecules. The first one is the attack of a MEMDO hydroxyl on a DPDM methoxy, which is shown in Figure 6a. The transition barrier is 14.0 kcal/mol. Parts b and c of Figure 6 show condensation reactions between two MEMDO hydroxyls and between one MEMDO hydroxyl and one MEMDO methoxy, respectively, with barriers of 18.7 and 19.8 kcal/mol. We find that condensation between one DPDM methoxy and one MEMDO hydroxyl has the largest reaction rate of 1.22×10^{-10} s^{-1}, thus in the third reaction step the process to produce the DPDM−MEMDO dimer as seen in Figure 7f is considered to be the most probable. The dimer can be also grown by condensation between a methoxy of a dimer DPDM site and a hydroxyl of a dimer MEMDO site, but its reaction is determined to have a smaller rate of 2.76×10^{-11} s^{-1} than that for the case between a DPDM methoxy and a

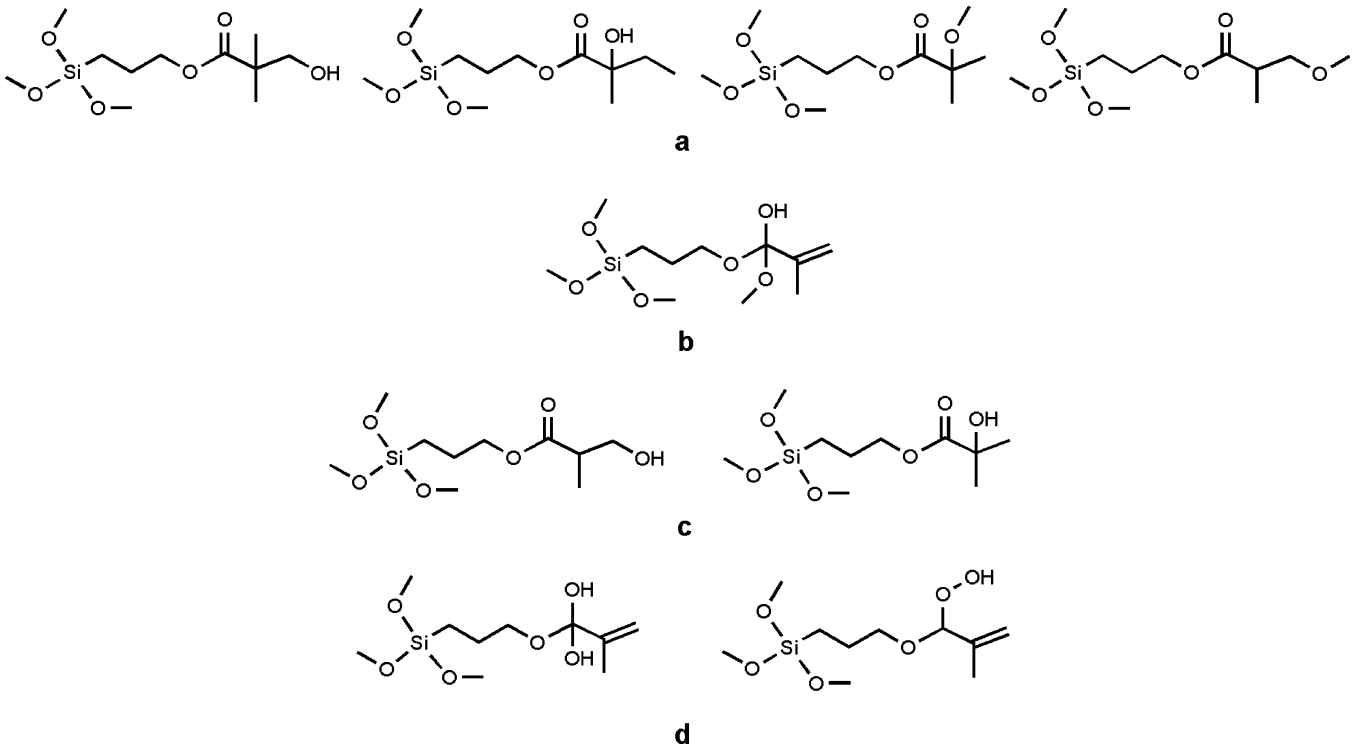

Figure 4. Products of H_2O or CH_3OH with a C═C or C═O of MEMO: (a) a CH_3OH with a C═C, (b) a CH_3OH with a C═O, (c) a H_2O with a C═C, and (d) a H_2O with a C═O.

MEMDO hydroxyl. Meanwhile, this rate is found to be slightly larger than the 1.17×10^{-11} s^{-1} for condensation between a hydroxyl of a dimer MEMDO site and a methoxy of a dimer MEMDO site. Here, it should be noted that the reaction rate on the larger nanostructures become smaller. This might be due to the increased geometry hindrance. Additionally, our SANS (small-scattering neutron scattering) measurements determine that the final products from the sol−gel reaction are mostly on the nanometer scale at sizes from 1.76 to 2.36 nm, which compare to the value of 2.01 nm determined on the elongated product by three dimers. The experimental size of the products is determined from the R_g (radius of gyration) of the products measured by SANS (small-angle neutron scattering). The products of the reaction between DPD (50 mol %) and MEMO (50 mol %) are solvated in 10 wt % acetone-d_6 to obtain accurate SANS results. Under this condition, R_g of the products is 0.68 nm. When the structure of the particle is spherical, the radius of the particle is $R = \sqrt{5/3}R_g$,, whereas the length of the rodlike particle is $L = \sqrt{12}R_g$. Consequently, the experimentally predicted size of the products is in the range of 1.76−2.36 nm.

B. Effects of H_2O on the Sol−Gel Reaction. H_2O can be released from the catalyst. The enthalpy of H_2O dissociation from the catalyst of $Ba(OH)_2 \cdot H_2O$ is calculated to be endothermic by 3.8 kcal/mol, whereas those from $Sr(OH)_2 \cdot H_2O$ and $Ca(OH)_2 \cdot H_2O$ are endothermic by 3.2 and 2.5 kcal/mol, respectively. Figure 8a describes a concerted H_2O attack on hydroxyl fragments of two DPDs by forming a six-centered structure that involves one H atom transfer from the H_2O to the DPD hydroxyl, bond dissociation of a Si−O bond to generate one H_2O molecule, one H atom transfer from the DPD OH to the attacking H_2O, and formation of a Si−O−Si bond. It is to be noted that H_2O participates in this reaction as a catalyst donating one hydrogen atom to the DPD hydroxyl and accepting one hydrogen atom from the other DPD hydroxyl simultaneously. The predicted barrier for this reaction is 16.9 kcal/mol with respect to an intermediate water complex formed from two DPD molecules, and this reaction is determined to be exothermic by 3.3 kcal/mol. Consequently, its predicted barrier and exothermic enthalpy indicate that the presence of H_2O included in the catalyst can significantly reduce the condensation rate between two DPDs. Before making a transition-state structure, H_2O and two DPD molecules form a water-mediated structure with a high exothermic enthalpy of 20.0 kcal/mol due to three hydrogen bonds between one hydrogen atom of the H_2O and the oxygen atom of a DPD hydroxyl, between one H atom of another DPD hydroxyl and the oxygen atom of the H_2O molecule, and between the hydrogen atom of one DPD and the oxygen atom of another DPD.

A concerted attack of the DPD on the MEMO in the presence of the H_2O is also described in Figure 8b, where the transition state is a six-centered ring structure. This step consists of several competing reactions. These are (1) one H atom transfer from the H_2O to the O atom of a Si−OCH_3 group in MEMO, (2) Si−OCH_3 bond dissociation, (3) one H atom transfer from the DPD hydroxyl to the H_2O, and (4) Si−O−Si bond formation. We obtain a transition-state barrier of 12.5 kcal/mol, and this process is found to be exothermic by 4.9 kcal/mol. The decreased barrier indicates that the presence of the catalyst can increase the condensation rate between one DPD and one MEMO, which is opposite to the case between two DPDs.

The H_2O effect on the switching reaction between DPD and MEMO is also explored. The transition state of this reaction is based on a six-centered ring structure as shown Figure 8c. The hydroxyl group of the catalyst H_2O attaches the MEMO silicon atom to form a Si−OH bond in the MEMO while one H_2O molecule is newly generated by bonding between the remaining H of the attacking water with a DPD hydroxyl. Simultaneously, a MEMO methoxy transfers to the DPD to replace the DPD hydroxyl with the methoxy group. The transition barrier for this case is 30.5 kcal/mol, which is higher than the cases of DPD with DPD and DPD with MEMO. Consequently, this result

TABLE 1: KMLYP/6-311+G(d,p)//B3LYP/6-31G Transition-State Barriers and Enthalpies for the Sol−Gel Processes Using DPD and MEMO Precursors[a]

sequence	reaction	barrier	enthalpy
	Condensation Reaction		
Step I			
	DPD OH + DPD OH → DPD-DPD + H_2O	14.9	−9.1
	DPD OH + MEMO OCH_3 → DPD−MEMO + CH_3OH[b]	15.1	−8.4
	DPD OH + MEMO OCH_3 → DPD−MEMO + CH_3OH[c]	73.1	−8.4
	MEMO OCH_3 + MEMO OCH_3 → MEMO-MEMO + $(CH_3)_2O$	69.3	−12.7
	Switching Reaction		
	DPD OH + MEMO OCH_3 → DPM + MEDO	6.9	−0.4
	Condensation Reaction		
Step II			
	DPM OH + DPM OH → DPM−DPM(I) + H_2O	18.5	−9.7
	DPM OH + DPM OCH_3 → DPM−DPM(II) + CH_3OH[d]	16.3	−8.3
	DPM OH + DPM OCH_3 → DPM−DPM(II) + CH_3OH[e]	68.5	−8.3
	DPM OCH_3 + DPM OCH_3 → DPM−DPM (III) + $(CH_3)_2O$	69.5	−11.9
	DPM OH + MEDO OH → DPM−MEDO(I) + H_2O[f]	15.8	−9.4
	DPM OH + MEDO OH → DPM−MEDO(I) + H_2O[g]	17.7	−9.4
	DPM OCH_3 + MEDO OH → DPM−MEDO(II) + CH_3OH[h]	16.2	−8.0
	DPM OCH_3 + MEDO OH → DPM−MEDO(II) + CH_3OH[i]	64.6	−8.0
	DPM OH + MEDO OCH_3 → DPM−MEDO(III) + CH_3OH[j]	12.1	−8.2
	DPM OH + MEDO OCH_3 → DPM−MEDO(III) + CH_3OH[k]	65.6	−8.2
	DPM OCH_3 + MEDO OCH_3 → DPM−MEDO(IV) + $(CH_3)_2O$[l]	59.9	−11.7
	DPM OCH_3 + MEDO OCH_3 → DPM−MEDO(IV) + $(CH_3)_2O$[m]	73.1	−11.7
	MEDO OH + MEDO OH → MEDO-MEDO(I) + H_2O	19.5	−9.0
	MEDO OH + MEDO OCH_3 → MEDO-MEDO(II) + CH_3OH[n]	16.8	−9.3
	MEDO OH + MEDO OCH_3 → MEDO-MEDO(II) + CH_3OH[o]	71.8	−9.3
	MEDO OCH_3 + MEDO OCH_3 → MEDO-MEDO(III) + $(CH_3)_2O$	68.2	−13.0
	Switching Reaction		
	DPM OH + MEDO OCH_3 → DPDM +MEMDO	8.5	−0.6
	Condensation Reaction		
Step III			
	DPDM OCH_3 + MEMDO OH → DPDM−MEMDO + CH_3OH	14.0	−7.6
	MEMDO OH + MEMDO OH → MEMDO-MEMDO(I) + H_2O	18.7	−9.1
	MEMDO OH + MEMDO OCH_3 → MEMDO-MEMDO(II) + CH_3OH	19.8	−8.3

[a] Energies are in units of kcal/mol. [b] DPD OH attack. [c] MEMO OCH_3 attack. [d] DPM OH attack. [e] DPM OCH_3 attack. [f] DPM OH attack. [g] MEDO OH attack. [h] MEDO OH attack. [i] DPM OCH_3 attack. [j] DPM OH attack. [k] MEDO OCH_3 attack. [l] DPM OCH_3 attack. [m] MEDO OCH_3 attack. [n] MEDO OH attack. [o] MEDO OCH_3 attack.

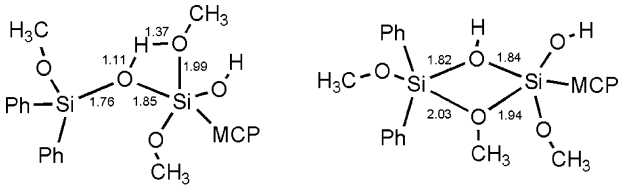

Figure 5. B3LYP/6-31G transition-state geometries for (a) condensation between a DPM hydroxyl and a MEDO methoxy and (b) switching between a DPM hydroxyl and a MEDO methoxy. Ph and MCP indicate phenyl and methacryloxypropyl groups, respectively. Bond lengths are in angstroms.

indicates that the final nanostructure could be modified by the presence of H_2O. This is because the H_2O released from the catalyst plays an important role in changing reaction pathways to modify the resulting product.

C. Vibrational Frequencies. We compute the frequencies of SiOH and $SiOCH_3$ fragments in the DPD, MEMO, DPM, and MEDO molecules at the B3LYP/6-31G level of theory using a scaling factor of 0.961.[40] The previous study[34] showed that the scaling factor for B3LYP frequencies to match with experimental values is closer to the scaling factor of unity than for the case with KMLYP. In this respect, we report only the vibrational frequencies obtained through the B3LYP calculations. The predicted frequency for a DPD Si−OH stretching mode is 648 cm^{-1}, whereas the frequency for a DPD SiO−H stretching mode is in the range of 3623−3621 cm^{-1}, which is consistent with experimental IR peaks[7,17,18] of 3600−3200 cm^{-1}. We also determine the frequencies of 561 and 1044 cm^{-1}, respectively, for MEMO Si−OCH_3 and SiO−CH_3 stretching modes. In addition, a C−H stretching mode of the MEMO $SiOCH_3$ is found to be in the range of 2921−2911 cm^{-1}. All frequencies in DPM and MEDO are similar to those in DPD and MEMO, which are shown in Table 2.

IV. Summary and Conclusions

Making the hybrid materials from the sol−gel reaction with nanometer-scale sizes is one interesting issue today. This is because the nanosizes of the resulting hybrid materials are useful for making fine nanostructures of optical waveguides and getting homogeneous properties within a waveguide. A first-principles calculation and experimental SANS measurement methods have been used to investigate the mechanism and the nanosize products of the sol−gel reaction using DPD and MEMO precursors. To determine the size of the products resulting from the sol−gel reaction, we have first explored the reaction mechanism by comparing the rates of all possible reactions at each step. It has been found that the switching reaction between a DPD hydroxyl and a MEMO methoxy having a kinetic reaction rate of 6.80×10^{-6} s^{-1} at room temperature, which generates one DPM and one MEDO as products, is the fastest process in the first reaction step. However, it has been determined that the reaction pathway can be modified by the presence of a catalyst such as $Ba(OH)_2 \cdot H_2O$ because the H_2O released from the catalyst changes the reaction barrier. In the second reaction step, we have also found that the switching

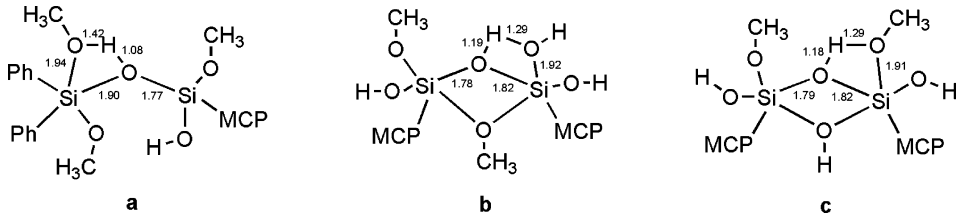

Figure 6. B3LYP/6-31G transition-state geometries for condensations between (a) a DPDM methoxy and a MEMDO hydroxyl, (b) two MEMDO hydroxyls, and (c) a MEMDO hydroxyl and a MEMDO methoxy. Ph and MCP indicate phenyl and methacryloxypropyl groups, respectively. Bond lengths are in angstroms.

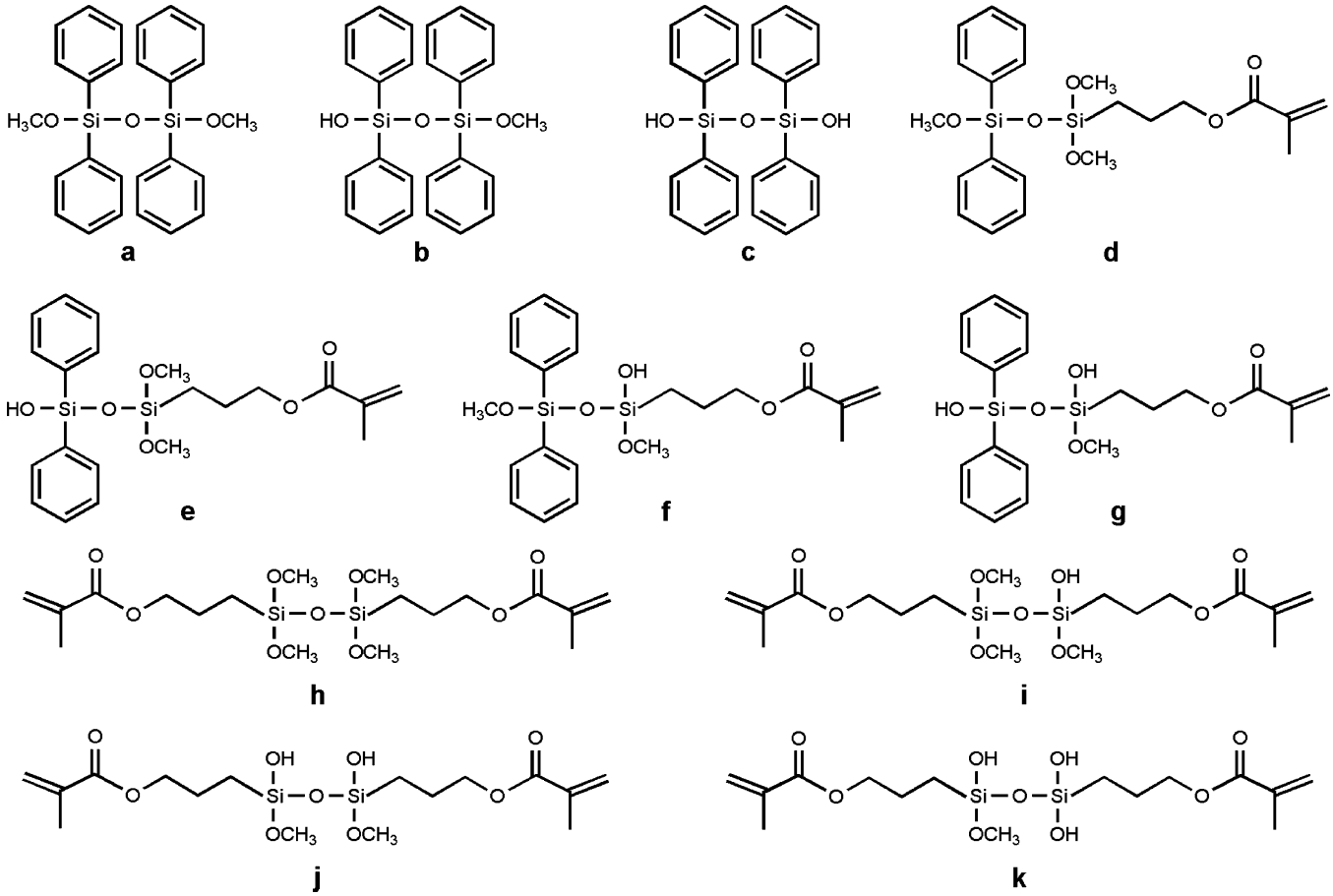

Figure 7. Products for condensations between (a) two DPM hydroxyls, (b) a DPM hydroxyl and a DPM methoxy, (c) two DPM methoxys (or two DPD hydroxyls), (d) one DPM hydroxyl and one MEDO hydroxyl, (e) one DPM methoxy and one MEDO hydroxyl (or one DPD hydroxyl and one MEMO methoxy), (f) one DPM hydroxyl and one MEDO methoxy (or one DPDM methoxy and MEMDO hydroxyl), (g) one DPM methoxy and one MEDO methoxy, (h) two MEDO hydroxyls (or two MEMO methoxys), (i) one MEDO hydroxyl and one MEDO methoxy, (j) two MEDO methoxys (or two MEMDO hydroxyls), and (k) one MEMDO hydroxyl and one MEMDO methoxy.

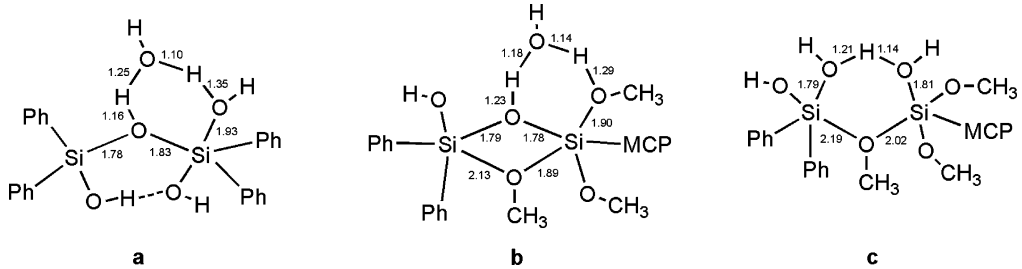

Figure 8. Catalytic effects of H_2O on transition states for (a) condensation between two DPDs, (b) condensation between a DPD hydroxyl and a MEMO methoxy, and (c) switching between a DPD hydroxyl and a MEMO methoxy. Ph and MCP indicate the phenyl group and methacryloxypropyl group, respectively. Bond lengths are in angstroms, where the B3LYP/6-31G geometries are used.

reaction between the DPM hydroxyl and the MEDO methoxy forming DPDM and MEMDO is the most favorable. This switching has a reaction rate of 4.61×10^{-7} s^{-1}. Next, the condensation between a methoxy of DPDM and a hydroxyl of MEMDO having a reaction rate of 1.22×10^{-10} s^{-1} has been determined to be most favorable in the third reaction step, which generates the DPDM−MEMDO dimer. In a similar fashion, additional growth has been found to occur by condensation between a methoxy of the dimer in the DPDM site and a hydroxyl of the dimer in the MEMDO site, which has a reaction

TABLE 2: Computed Frequencies of Various Stretching Modes for SiOH and $SiOCH_3$ of DPD, MEMO, DPM, and MEDO at the B3LYP/6-31G Level with a Scaling Factor of 0.961[a]

molecule	Si−OH	SiO−H	Si−OCH_3	SiO−CH_3	SiOC−H_3
DPD	648	3623			
		3621			
MEMO			561	1044	2921
					2913
					2911
DPM	695	3621	712	1037	2911
MEDO	647	3644	570	1058	2922
				1052	2912
				1045	
		3600−3200[b]			2840[b]

[a] Frequencies in units of cm^{-1}. [b] Experimental values taken from ref 7.

rate of 2.76×10^{-11} s^{-1}. In addition, our SANS measurements have shown that the final products for the sol−gel reaction are on the nanometer scale at sizes of 1.76−2.36 nm, which compare to the size of 2.01 nm for the elongated structure by three dimers. This result implies that the reaction rate on the larger nanostructures become negligibly small. Additionally, the computed frequencies of SiOH and $SiOCH_3$ of DPD, MEMO, DPM, and MEDO have been discussed.

Acknowledgment. The computational resources at the Materials and Process Simulation Center (MSC) at the California Institute of Technology and Korea Advanced Institute of Science and Technology have been supported by grants from NSF-MRI and ARO-DURIP and by a SUR grant from IBM. We also appreciate the financial support from the interdisciplinary research program and the Center for Ultramicrochemical Process Systems (CUPS) sponsored by KOSEF (2005).

References and Notes

(1) Okoshi, M.; Kuramatsu, M.; Inoue, N. *Appl. Phys. Lett.* **2002**, *81*, 789.
(2) Zhang, L.; Xie, W.; Wu, Y.; Xing, H.; Li, A.; Zheng, W.; Zhang, Y. *Opt. Mater.* **2003**, *22*, 283.
(3) Koo, J. S.; Smith, P. G. R.; Williams, R. B.; Riziotis, C.; Grossel, M. C. *Opt. Mater.* **2003**, *23*, 583.
(4) Hikita, M.; Yoshimura, R.; Usui, M.; Tomaru, S.; Imamura, S. *Thin Solid Films* **1998**, *331*, 303.
(5) Coudray, P.; Chisham, J.; Malek-Tabrizi, A.; Li, C.-Y.; Andrews, M. P.; Peyghambarian, N.; Najafi, S. I. *Opt. Commun.* **1996**, *128*, 19.
(6) Najafi, S. I.; Touam, T.; Sara, R.; Andrews, M. P.; Fardad, M. A. *J. Lightwave Technol.* **1998**, *16*, 1640.
(7) Buestrich, R.; Kahlenberg, F.; Popall, M.; Dannberg, P.; Müller-Fiedler, R.; Rösch, O. *J. Sol.-Gel Sci. Technol.* **2001**, *20*, 181.
(8) Hay, J. N.; Raval, H. M. *Chem. Mater.* **2001**, *13*, 3396.
(9) Bourget, L.; Corriu, R. J. P.; Leclercq, D.; Mutin, P. H.; Vioux, A. *J. Non-Cryst. Solids* **1998**, *242*, 81.
(10) Bourget, L.; Leclercq, D.; Vioux, A. *J. Sol.-Gel Sci. Technol.* **1999**, *14*, 137.
(11) Hay, J. N.; Porter, D.; Raval, H. M. *J. Mater. Chem.* **2000**, *10*, 1811.
(12) Loy, D. A.; Shea, K. J. *Chem. Rev.* **1995**, *95*, 1431.
(13) Mark, J. E. *Polym. Eng. Sci.* **1996**, *36*, 2905.
(14) Haas, K. H. *Adv. Eng. Mater.* **2000**, *2*, 571.
(15) Sanchez, C.; Ribot, F. *New. J. Chem.* **1994**, *18*, 1007.
(16) Judeinstein, P.; Sanchez, C. *J. Mater. Chem.* **1996**, *6*, 511.
(17) Houbertz, R.; Fröhlich, L.; Popall, M.; Streppel, U.; Dannberg, P.; Bräuer, A.; Serbin, J.; Chichkov, B. N. *Adv. Eng. Mater.* **2003**, *5*, 551.
(18) Houbertz, R.; Domann, G.; Cronauer, C.; Schmitt, A.; Martin, H.; Park, J.-U.; Fröhlich, L.; Buestrich, R.; Popall, M.; Streppel, U.; Dannberg, P.; Wächter, C.; Bräuer, A. *Thin Solid Films* **2003**, *442*, 194.
(19) Hench, L. L.; West, J. K. *Chem. Rev.* **1990**, *90*, 33.
(20) Becke, A. D. *J. Chem. Phys.* **1993**, *98*, 5648.
(21) Kang, J. K.; Musgrave, C. B. *J. Chem. Phys.* **2001**, *115*, 11040.
(22) Pople, J. A.; Head-Gordon, M.; Raghavachari, K. *J. Chem. Phys.* **1987**, *87*, 5968.
(23) Kang, J. K.; Musgrave, C. B. *J. Chem. Phys.* **2002**, *116*, 275.
(24) McIntosh, R.; Kuan, T. S.; Defresart, E. *J. Electron. Mater.* **1992**, *21*, 57.
(25) Garofalini, S. H. *J. Non-Cryst. Solids* **1990**, *120*, 1.
(26) Becke, A. D. *J. Chem. Phys.* **1986**, *85*, 7184.
(27) Perdew, J. P. *Phys. Rev. B* **1986**, *33*, 8822.
(28) Becke, A. D. *Phys. Rev. A* **1988**, *38*, 3098.
(29) Gill, P. M. W. *Mol. Phys.* **1996**, *89*, 433.
(30) Perdew, J. P.; Burke, K.; Ernzerhof, M. *Phys. Rev. Lett.* **1996**, *77*, 3865.
(31) Slater, J. C. *Quantum Theory of Molecules and Solids* McGraw-Hill: New York, 1974; Vol. 4.
(32) Vosko, S. H.; Wilk, L.; Nusair, M. *Can. J. Phys.* **1980**, *58*, 1200.
(33) Kang, J. K.; Musgrave, C. B. *J. Appl. Phys.* **2002**, *91*, 3408.
(34) Kang, J. K.; Musgrave, C. B. *J. Chem. Phys.* **2002**, *116*, 9907.
(35) McLean, A. D.; Chandler, G. S. *J. Chem. Phys.* **1980**, *72*, 5639. Ditchfield, R.; Hehre, W. J.; Pople, J. A. *J. Chem. Phys.* **1971**, *54*, 724. Frisch, M. J.; Pople, J. A.; Binkley, J. S. *J. Chem. Phys.* **1984**, *80*, 3265.
(36) Frisch, M. J.; Trucks, G. W.; Schlegel, H. B.; Scuseria, G. E.; Robb, M. A.; Cheeseman, J. R.; Montgomery, J. A., Jr.; Vreven, T.; Kudin, K. N.; Burant, J. C.; Millam, J. M.; Iyengar, S. S.; Tomasi, J.; Barone, V.; Mennucci, B.; Cossi, M.; Scalmani, G.; Rega, N.; Petersson, G. A.; Nakatsuji, H.; Hada, M.; Ehara, M.; Toyota, K.; Fukuda, R.; Hasegawa, J.; Ishida, M.; Nakajima, T.; Honda, Y.; Kita, O.; Nakai, H.; Klene, M.; Li, X.; Knox, J. E.; Hratchian, H. P.; Cro, J. B.; Adamo, C.; Jaramillo, J.; Gomperts, R.; Stratmann, R. E.; Yazyev, O.; Austin, A. J.; Cammi, R.; Pomelli, C.; Ochterski, J. W.; Ayala, P. Y.; Morokuma, K.; Voth, G. A.; Salvador, P.; Dannenberg, J. J.; Zakrzewski, V. G.; Dapprich, S.; Daniels, A. D.; Strain, M. C.; Farkas, O.; Malick, D. K.; Rabuck, A. D.; Raghavachari, K.; Foresman, J. B.; Ortiz, J. V.; Cui, Q.; Baboul, A. G.; Clifford, S.; Cioslowski, J.; Stefanov, B. B.; Liu, G.; Liashenko, A.; Piskorz, P.; Komaromi, I.; Martin, R. L.; Fox, D. J.; Keith, T.; Al-Laham, M. A.; Peng, C. Y.; Nanayakkara, A.; Challacombe, M.; Gill, P. M. W.; Johnson, B.; Chen, W.; Wong, M. W.; Gonzalez, C.; Pople, J. A. *Gaussian 03*; Gaussian, Inc.: Pittsburgh, PA, 2003.
(37) Fawcett, J. K.; Camerman, N.; Camerman, A. *Can. J. Chem.* **1977**, *55*, 3631.
(38) Párkányi, L.; Bocelli, G. *Cryst. Struct. Commun.* **1978**, *7*, 335.
(39) Laidler, K. J. *Chemical Kinetics*; McGraw-Hill: New York, 1950; Chapter 3.
(40) Foresman, J. B.; Frisch, A. E. *Exploring Chemistry with Electronic Structure Methods*, 2nd ed.; Gaussian, Inc.: Pittsburgh, PA, 2000.